IEEE Access
Multidisciplinary | Rapid Review | Open Access Journal

Received November 15, 2021, accepted November 28, 2021, date of publication November 30, 2021,
date of current version December 8, 2021.

Digital Object Identifier 10.1109/ACCESS.2021.3131559

Dynamics of Mechanical Automatic Vertical Drilling System With a Novel Hydraulic Balanced Turbine

JIN WANG[1,2], QILONG XUE[1,2], BAOLIN LIU[1,2], FANGTAO LI[1,2], YANBIN ZANG[3], AND LIN CHAI[1,2]

[1]School of Engineering and Technology, China University of Geosciences, Beijing 100083, China
[2]Key Laboratory of Deep Geodrilling Technology, Ministry of Land and Resources, Beijing 100083, China
[3]Sinopec Research Institute of Petroleum Engineering, Beijing 1000101, China

Corresponding author: Qilong Xue (xql@cugb.edu.cn)

This work was supported in part by the Natural Science Foundation of China under Grant 42072341, and in part by the Fundamental Research Funds for the Central Universities under Grant 2-9-2018-096.

ABSTRACT The automatic vertical drilling system (VDS) adopts downhole closed-loop control, through ground monitoring, a large closed-loop control on the ground and downhole is formed to keep the wellbore in a vertical position. The Mechanical Automatic Vertical Drilling System (MVDS) which working in full mechanical mode has been more economical, safety and reliability. We proposed and developed a novel MVDS with high control accuracy in this paper. A new type of Hydraulic Balance Turbine (HBT) is presented and applied to MVDS, used to drive the upper disc valve to reduce the frictional resistance and the influence of the bottom drilling tool vibration. This can achieve a ''soft'' connection between eccentric platform and the upper valves, eliminate the effect of the friction between the upper valve and the lower valve, and optimize the control ability. After HBT optimization, the stable angle is closer to the low side, which can make the control of MVDS more accurate. The same conclusion was verified by laboratory tests as well.

INDEX TERMS Dynamics, eccentric platform, hydraulic balanced turbine, simulation, vertical drilling system.

I. INTRODUCTION

In oil and gas drilling, boreholes typically tend to penetrate bedding planes and other geological features at a right angle without special drilling procedures or technology. In addition to natural drift, drilling practices can also create boreholes with doglegs or other irregularities in shape or direction. In the past, passive deviation control technologies [1]–[3] such as tower drilling tools, pendulum assemblies and full hole drilling tools were run to maintain low borehole inclination angles, but they offered limited effectiveness in hard or steeply dipping formations. Correction runs to bring the borehole back to vertical were costly and did nothing to prevent the problem from recurring. Kontinentales Tiefbohr programm der Bundesrepublik Deutschland (KTB), the German Continental Deep Drilling Program [4], [5], drilled a 9101m (29860-ft) vertical well to study fundamental aspects of the Earth's crust. An automatic vertical drilling system (VDS) limited building angle and minimized hole size and friction. The vertical drilling technology adopts downhole closed-loop control [6], which programmed on surface to automatically and capable of preventing boreholes from vertical and can also return inclined boreholes to verticality. The advantages of the VDS include precise well placement, high-quality boreholes, high Rate of Penetration (ROP), and effective hole cleaning Bratton *et al.* [7]. Although vertical drilling may seem relatively simple, it can present challenges similar to directional drilling, and it is required in some of the most expensive operating arenas, such as subsalt development in deep water. Vertical drilling is also critical to the success of extended-reach drilling operations. Excessive tortuosity in the top hole causes increased torque and drag in subsequent hole sections, which can lead to wear of drill pipe and casing. Tortuosity also increases the potential for drilling problems, such as poor hole cleaning, stick/slip and inability to reach planned depth because of torque and drag. Currently, there are mainly three kinds of typical VDS tools, including the Baker Hughes Verti-Trak system, Schlumberger Power-V system,

The associate editor coordinating the review of this manuscript and approving it for publication was Agustin Leobardo Herrera-May.

This work is licensed under a Creative Commons Attribution 4.0 License. For more information, see https://creativecommons.org/licenses/by/4.0/

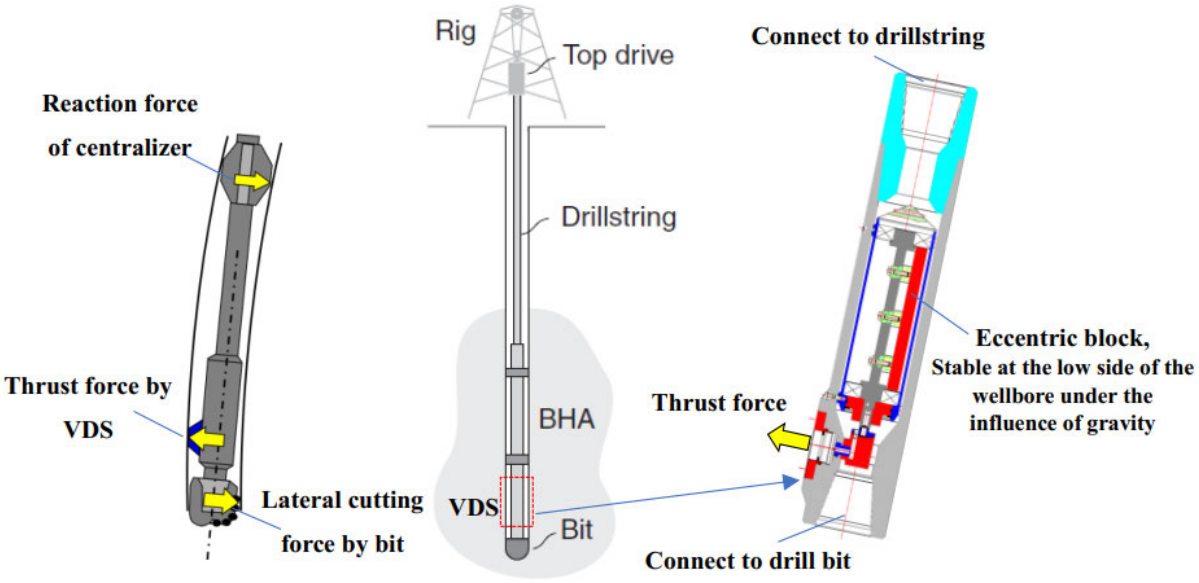

(a) Schematic of a drilling system for a vertical borehole configuration

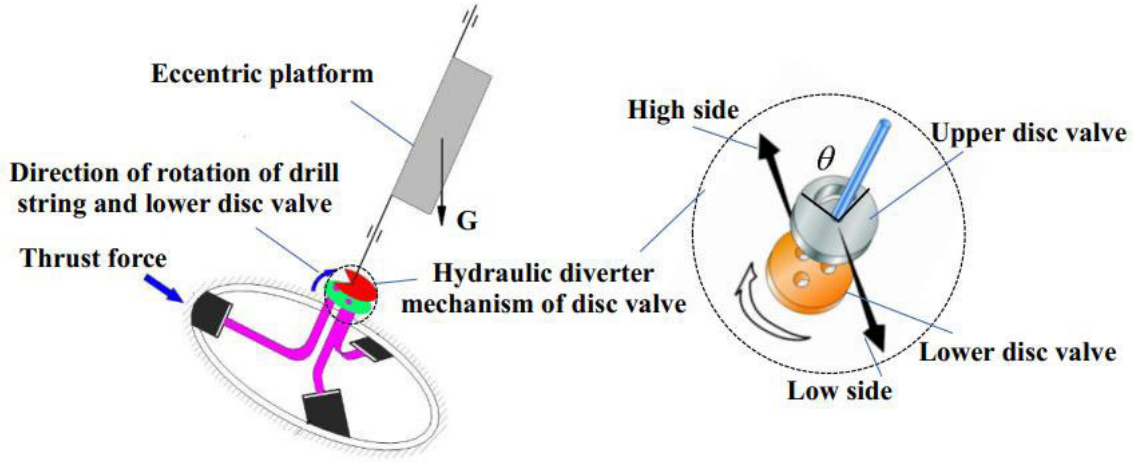

(b) Schematic of working principle of MVDS

FIGURE 1. Schematic of a drilling system for a vertical borehole configuration (a) and the working principle of MVDS (b), When the VDS works, it will generate a pushing force to push against the high side of the wellbore and then return inclined boreholes to verticality. The eccentric block turn to the low side of the hole under the action of gravity, drives the upper disc valve to stabilize in the expected position. Due to the lower disc valve rotates with the bottom hole drilling tool, when one of its three valve holes rotates to the upper disc valve hole, the corresponding hydraulic flow channel is connected and pushed the pads to the high side of the borehole.

Halliburton Sperry-sun V-Pilot system [2], [6], [8]. All of them have sensitive and expensive electronic components [9] which has low reliability under complex conditions such as high temperature (more than 200°) and extreme vibration in ultra-deep wells [10]–[13].

In recent years, the Mechanical Automatic Vertical Drilling System (MVDS) [14]–[16] which working in full mechanical mode and more economical, safety and reliability has gradually attracted attention. Especially in today's low oil price economic situation [17], it has become the best choice for ''deviation control and fast drilling''. The working principle of MVDS as shown in Fig.1, (a) is the schematic of a drilling system for a vertical borehole configuration, When the VDS works, it will generate a pushing force to push against the high side of the wellbore and then return inclined boreholes to verticality. In MVDS, as show in the Fig.1 (a) and (b), there has an eccentric block, which could stable at the low side of the wellbore under the influence of gravity. When the borehole and drilling tool is inclined, the eccentric block turns to the low side of the hole under the action of gravity, which drives the upper disc valve to stabilize in the expected position. The lower disc valve rotates with the bottom hole drilling tool and the drill bit. When one of its three valve holes rotates to the upper disc valve hole, the corresponding hydraulic flow

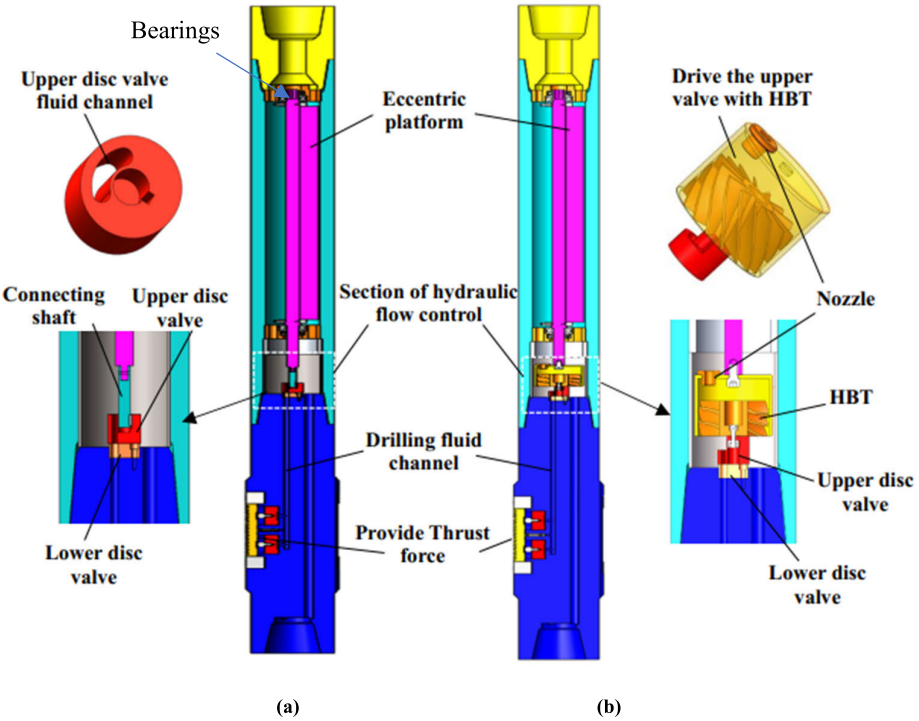

FIGURE 2. Two design of MVDS, (a) Original design; (b) New design. In the new design, the eccentric platform control the up disc valve with a nozzle to drive the HBT stable in the low direction of the wellbore, then the vibration of the tool caused by pads will not affect the stability of the eccentric platform. The "soft" connection between the eccentric platform and the upper disc valve is realized.

channel is connected. The pads will be pushed to the high side of the borehole by internal and external drilling fluid differential pressure. After a period of time, it is turned off, the next one is turned on, and in this way the full-rotation dynamic correction is realized. Eccentric platforms as shown in Fig.1(b) are now widely applied in MVDS. However, due to the friction between the upper and lower valves, as well as the vibration caused by bottom hole assembly [18], [19], the well deviation control accuracy is low, which is a key factor to restrict the development of MVDS.

In this paper, a novel Hydraulic Balance Turbine (HBT) is installed at MVDS, the balance moment generated by the HBT is used to stabilize the upper disc valve at a predetermined position. This can achieve a ''soft'' connection between eccentric platform and the upper valves, eliminate the effect of the friction between the upper valve and the lower valve, and optimize the valve control ability. Therefore, deviation precision will be improved greatly.

The paper is organized as follows. The conceptual design and geometric features of the new turbine using MVDS are presented in Section 2. Subsequently in Section 3, the mechanical model of HBT and the mathematical methods of simulation based on FE methods is presented. Then, the mathematical model of dynamic characteristics of eccentric block torsion is established. Next, the main results of the paper are given in Section 4, the dynamic characteristics of eccentric block torsion and the optimization effect of HBT were obtained. Finally, Section 5 draws conclusions and gives a summary of the most important outcomes of this work with suggestions for the future work.

II. NOVEL HBT IN MECHANICAL VERTICAL DRILLING TOOLS

In MVDS, because of the friction resistance between the upper and lower disc valves and the vibration of the bottom drilling tool [18], [19], the deviation control accuracy of the MVDS is difficult to improve, which has become the main factor restricting its development. The main factors affecting the accuracy of deviation control are as follows: firstly, due to the friction resistance of the upper and lower disc valves, the eccentric platform cannot be stabilized at the low side of the well [15]; Secondly, the centralized force of the pads cannot be stabilized at the high side of the well due to the vibration of the bottom drillstring [20]–[23].

In addition to the friction resistance between the upper and lower disc valves, the friction resistance between the mechanical structures, bearings and the damp effect of drilling fluid [24] will also affect the platform, but the friction resistance between the upper and lower disc valves is the most significant, and it is difficult to quantify and compensate the friction resistance at the beginning of the design due to the influence of bottom drilling tool dynamics [18], [25].

In this paper, a novel HBT is installed at MVDS as shown in Fig.2 (b), the balance moment generated by the HBT is used to stabilize the upper disc valve at a predetermined position. The eccentric platform is only controlled by the

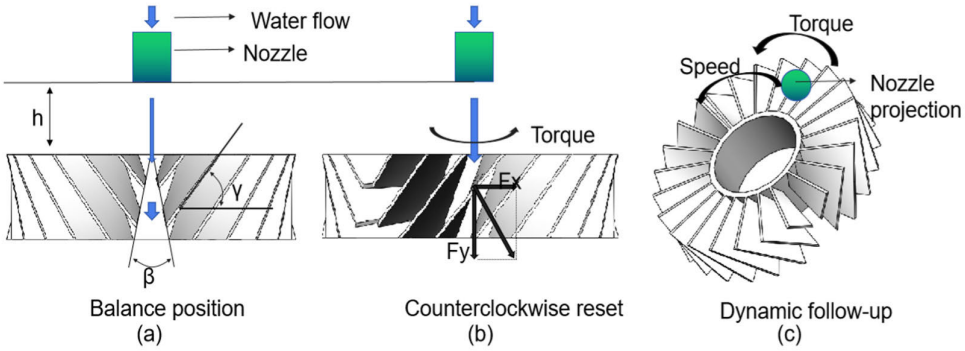

FIGURE 3. Working principle of the HBT, (a) shows the nozzle and the turbine in a balance position, and the nozzle impact distance is h, turbine blade relative angle is β; (b) shows a kind of unbalanced state of HBT, fluid produces torque (Clockwise or counterclockwise) through the nozzle; (c) shows the dynamic following performance of the HBT with the speed of nozzle.

liquid flow nozzle to drive the HBT. The "soft" connection between the eccentric platform and the upper disc valve is realized, so that the eccentric platform is not affected by the friction resistance of the upper and lower disc valve, and the abnormal oscillation of the eccentric platform will not be transmitted to the upper disc valve, which makes the thrust force as shown in fig.1 (a) more stable. The HBT optimizes the performance of the control mechanism of MVDS. The advantages as following two aspects: firstly, it effectively avoids the influence of the frictional resistance of the upper and lower disc valves, as well as the influence of stick-slip vibration of the bottom drilling tools [18]; secondly, utilizing the follow-up and hysteresis characteristics of the HBT, can cushion the vibration of the eccentric block, effectively reduce the influence of the swing of the eccentric block on the upper plate valve, and improve the stability of the control. As shown in Fig.2, the hydraulic turbine is installed between the upper and lower disc valves, the hydraulic impact of the nozzle provides the driving force.

The working principle of the HBT is shown in Fig. 3, where (a) depicts the balance state of the turbine, where the turbine torque is balanced and the turbine is stable. When the nozzle moves to other positions driven by the control mechanism, the hydraulic impact of the nozzle will provide the driving torque, as shown in Fig. 3 (b). Finally, the turbine will restore to its balance position under the action of the torque produced by the hydraulic impact of the nozzle. Turbine and upper disc valve are fixed together, which drives the movement of upper disc valve and realizes the flow channel control of upper and lower disc valve.

Under the impact of nozzle jet, the turbine overcomes the frictional resistance torque and then moves. The ability of the hydraulic turbine to overcome the frictional resistance torque is called the start-up performance of the turbine. When the nozzle moves driven by the eccentric platform, the turbine will move along with the nozzle, as shown in the Fig.1 (c). We call this characteristic of the turbine dynamic following performance. When the nozzle deviates from the balance position, the turbine will gradually stabilize at the position shown in Fig. 3 (a). At this time, the hydraulic moment tends to be balanced. The anti-disturbance performance of the turbine is defined as the dynamic balancing performance of the HBT. Whether the turbine can overcome frictional resistance and follow the nozzle rotation depends on the turbine torque. This paper studies the factors affecting the turbine impact torque, and provides a theoretical basis for the optimal design of the balance turbine.

III. MODELING AND METHODS

A. MODELING OF ECCENTRIC PLATFORM

1) STATIC ANALYSIS OF ECCENTRIC PLATFORM

When the inclination angle of the well exists, the eccentric block will generate an eccentric torque that always points to the low side of the well. As shown in the Fig.4, let F_E is the eccentric force of the eccentric block during the movement. Gravity G produces two components for an eccentric block, F_r and F_a. The component F_E of F_r generates an eccentric force, thereby providing an eccentric torque. The eccentric torque T_E will be calculated by the following:

$$G = \rho g \mathrm{V} = \frac{\pi}{2}\rho g l\left(r_2^2 - r_1^2\right) \tag{1}$$

$$F_r = G sin\beta \tag{2}$$

$$F_E = G sin\beta sin\phi \tag{3}$$

$$T_E = \frac{2}{3}\rho g l\left(r_2^3 - r_1^3\right) sin\beta sin\phi \tag{4}$$

wherein, r_1 and r_2 are inside and outside radius of eccentric block, m; ρ is the material density of the eccentric block, kg/m^3; g is gravitational acceleration, 9.8m/s^2; l is the length of the eccentric block, m.

Friction resistance torque comes mainly from two aspects: One is the frictional resistance torque generated by axial and radial bearings; The second is the frictional resistance caused by the relative rotation of the upper and lower disc valves. Assuming that the radial bearing friction is F_{TB}, the axial thrust bearing friction is F_{AB}, and the relative motion

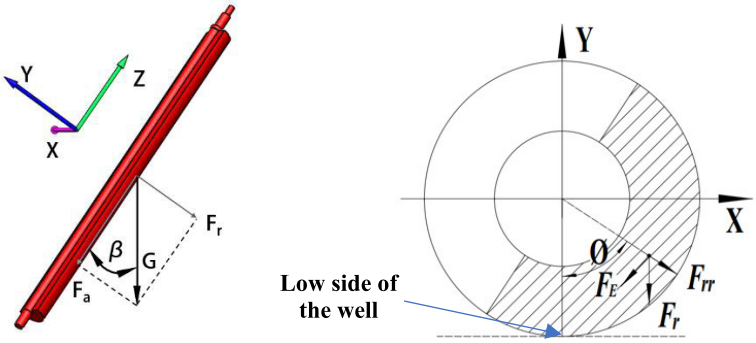

FIGURE 4. Calculation model of eccentric torque of eccentric block, the angle between the eccentric block and the vertical direction is β, and the angle between the symmetrical centerline of the eccentric block and the low side of the wellbore is ϕ. Gravity G produces two components for an eccentric block, F_r and F_a. The component F_E of F_r generates an eccentric force, thereby providing an eccentric torque.

resistance of the disc valve is F_P, all frictional resistance directions are always opposite to the direction of the tool's movement. Axial component $F_a = G\cos\beta$ and radial component $F_{rr} = G\sin\beta\cos\phi$ of the eccentric block gravity will be provided to the axial and radial bearings positive pressure respectively. The resistance torque generated by the bearings are calculated as follows [15]:

$$F_{TB} = G\sin\beta\cos\phi\mu_{TB} \tag{5}$$

$$F_{AB} = G\cos\beta\mu_{AB} \tag{6}$$

$$T_{TB} = \frac{\pi}{2}\rho g l\left(r_2^2 - r_1^2\right)\sin\beta\cos\phi\mu_{TB}r_{TB} \tag{7}$$

$$T_{AB} = \frac{\pi}{2}\rho g l\left(r_2^2 - r_1^2\right)\cos\beta\mu_{AB}r_{AB} \tag{8}$$

wherein r_{TB} is the radial bearing equivalent radius, m; r_{AB} is equivalent radius of axial thrust bearing, m.

Without driving the upper valve, if $T_E > T_{TB} + T_{AB}$, the eccentric block will turn to the lower side of the wellbore, in fact, the frictional resistance of the disc valve is the main factor. As shown in the Fig.5, because the upper disc valve has an arc hole for overcurrent, we divide the friction torque into three parts, the area of S_1 and S_2 was ignored during the calculation and the calculation formula as follows:

$$\begin{cases} T_{P1} = \int_0^{R_1} \mu_P P_l 2\pi R^2 dR = \frac{2}{3}\pi\mu_p P_l R_1^3 & 0 \le R_c \le R_1 \\ T_{P2} = \frac{\alpha}{2\pi}\frac{2}{3}\pi\mu_P P_l\left(R_2^3 - R_1^3\right) \\ = \frac{\alpha}{3}\mu_P P_l\left(R_2^3 - R_1^3\right) & R_1 < R_c < R_2 \\ T_{P3} = \frac{2}{3}\pi\mu_P P_l\left(\left(\frac{D}{2}\right)^3 - R_2^3\right) & R_2 \le R_c \le D/2 \end{cases} \tag{9}$$

wherein D is outer diameter of upper disc valve, mm; μ_P is coefficient of friction between disc valves; α is opening angle of arc hole of upper disc valve; P_l is the pressure on the upper disc valve during drilling fluid flow.

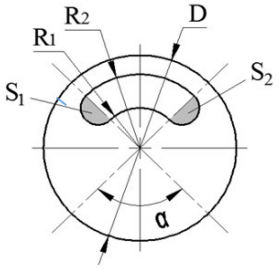

FIGURE 5. Schematic of upper disk valve structure.

Then the total frictional torque between the upper and lower disc valves is,

$$T_P = T_{P1} + T_{P2} + T_{P3} \tag{10}$$

The formula for calculating the friction torque T_P between disk valves can also be simplified as:

$$T_P = P_l \cdot S_P \cdot R_d \cdot \mu_P \tag{11}$$

wherein is the S_P is the area of disc valve except circular hole, also is the area of effect of fluid pressure differential, $S = \pi R_1^2 + \frac{2\pi-\alpha}{2}(R_2^2 - R_1^2) + \pi((\frac{D}{2})^2 - R_2^2)$, m^2; R_D is the equivalent friction radius of disc valve, m.

In the process of working operation of MVDS, if the eccentric block can reliably move to the lower side of the wellbore, need to satisfy the following:

$$T_E > T_{TB} + T_{AB} + T_P \tag{12}$$

2) DYNAMICS OF ECCENTRIC PLATFORM

Assuming the equivalent total frictional resistance is F_f, R_T is the equivalent friction radius. Obviously, total friction torque $T_f = F_f R_T = T_{TB} + T_{AB} + T_P$, combine Equation (7)-(10),

$$F_f = \frac{G\sin\beta\cos\phi\mu_{TB}r_{TB} + G\cos\beta\mu_{AB}r_{AB} + F_P\mu_P r_{db}}{R_T} \tag{13}$$

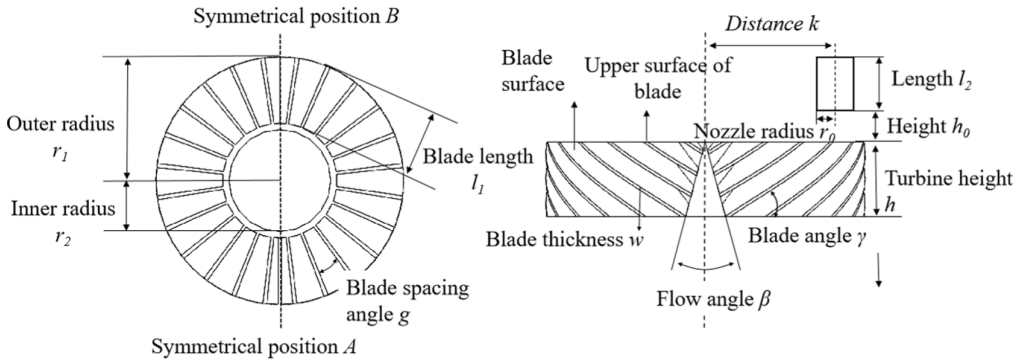

FIGURE 6. Turbine schematic diagram and the main parameters, the design parameters of balance turbine include outer radius of turbine r_1, inner radius of turbine r_2, turbine height h, flow angle of turbine β, blade length l_1, blade angle γ, blade spacing angle g, blade number n, blade thickness w, nozzle radius r_0, nozzle length l_2, nozzle height h_0, and nozzle distance k from the center.

wherein R_T can be considered as the distance from the centroid of the eccentric block to the center of rotation, can be expressed as follows:

$$r = \frac{4(r_2^2 + r_2 r_1 + r_1^2)}{3\pi(r_2 + r_1)} \tag{14}$$

The direction of the friction resistance depends on the relative movement direction of the eccentric platform and the tool body, so the direction of the friction force is always opposite to the direction of the eccentric force. The motion of the eccentric platform can be expressed as:

$$F_E - F_f = mR_T\ddot{\phi} \tag{15}$$

wherein m is the mass of the eccentric block, $m = G/g$. $\ddot{\phi}$ is the angular acceleration. Substituting formulas (3) and (13) to (15) can be obtained:

$$\frac{G}{g}R_T^2\ddot{\phi} - Gsin\beta(R_T sin\phi - \cos\phi\mu_{TB}r_{TB}) - (G\cos\beta\mu_{AB}r_{AB} + F_P\mu_P r_{db}) = 0 \tag{16}$$

According to the different movement modes of the eccentric platform, Equation (15) can be rewritten as follows:

$$\begin{cases} -F_E + F_f = -mR_T\ddot{\phi} & \omega_t \geq \omega_e, \sin\phi \geq 0 \\ -F_E - F_f = -mR_T\ddot{\phi} & \omega_t < \omega_e, \sin\phi \geq 0 \\ F_E + F_f = mR_T\ddot{\phi} & \omega_t \geq \omega_e, \sin\phi < 0 \\ F_E - F_f = mR_T\ddot{\phi} & \omega_t < \omega_e, \sin\phi < 0 \end{cases} \tag{17}$$

wherein ω_t is the rotary angular velocity of drillstring; ω_e is the rotational angular velocity of eccentric platform.

The eccentric platform will eventually stabilize at an angle ϕ_s, which we call the stable angle. At the stable angle position, the eccentric force and the friction force meet the opposite direction and have the same magnitude. It can be seen that the larger the eccentric force or the smaller the friction, the smaller the stability angle. Therefore, in the design process, the friction should be reduced as much as possible to improve the control accuracy of the drilling tool.

In this paper, the classical Coulomb friction model is used to analyze the dynamics of eccentric platform. The classic Coulomb model states that the friction force F_f can be calculated as,

$$F_f = -\mu_0 W\dot{v}_t / \|\dot{v}_t\| \tag{18}$$

where μ_0 is universal representation of any coefficient of friction, W is the magnitude of the normal contact force and $\dot{v}_t$ is the tangential contact velocity. Obviously, this friction model will be scale invariant if is scale F_f independent.

B. NUMERICAL SIMULATION MODEL OF HBT

To verify the feasibility of the new design of this paper, the three-dimensional analysis model of HBT is established in software of Solidworks. Conventional turbine design is complex [27]–[29], in order to make the design of the turbine simple and efficient, projection modeling method is used for the blade. The blade profile is only controlled by the outer angle of the blade. The design parameters of HBT as shown in Fig.6, include blade angle γ, blade number n, blade thickness w, blade length l_1, turbine height h and so on.

The working medium of the turbine is liquid. Generally, the liquid is regarded as an incompressible fluid. A flowing fluid follows the law of conservation of mass, momentum and energy. However, it is very difficult to solve the velocity field and pressure field in complex flows accurately. The computational fluid dynamics (CFD) method can be used to solve the approximate solution to satisfy the engineering application. The accuracy of CFD methods has been verified in many fields. This paper employed numerical simulation tools to demonstrate the results of the theoretical analysis, and to study the variation of geometric parameters.

The steady operating performance of the turbine was evaluated using a set of dimensionless coefficients which are characterized in terms of the torque coefficient C_t, input power coefficient f_i, turbine efficiency δ and flow coefficient φ. The definitions related to these parameters are expressed

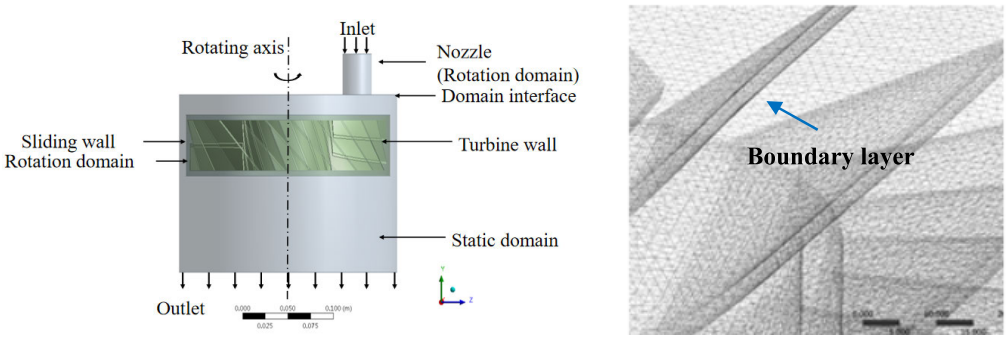

(a) simulation model (b) section mesh of the model

FIGURE 7. Three-dimensional simulation model and meshing, (a) in the simulation model, the balance turbine is installed in the fluid environment simulating the actual drilling tool, (b) shows a partial enlargement of the meshing in the ANSYS.

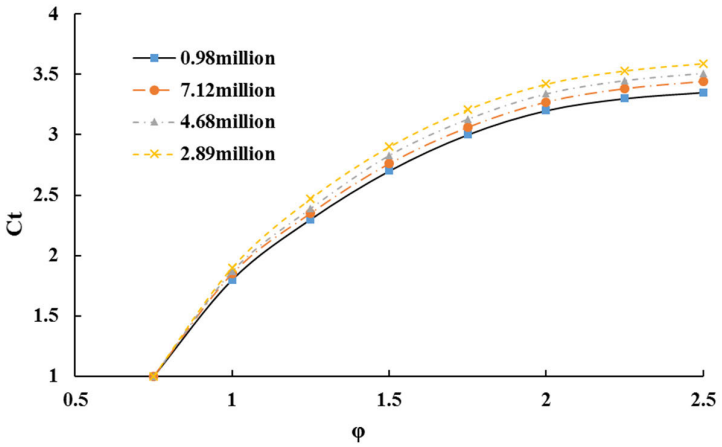

FIGURE 8. Mesh independency study (C_t-φ).

as follows:

$$C_t = 2T_o / \left\{ \rho(v_r^2 + u_r^2) \cdot n \cdot \frac{r_1 + r_2}{2} s \right\} \tag{19}$$

$$f_i = 2\Delta PQ / \left\{ \rho(v_r^2 + u_r^2) s n v_r \right\} \tag{20}$$

$$\eta = T_o \omega / (\Delta p Q) = C_t / (f_i \varphi) \tag{21}$$

$$\varphi = v_r / u_r \tag{22}$$

where ΔP is the total pressure drop between the inlet and outlet of the turbine; T_o is the output torque; and Q and ρ denote the air volumetric flow rate and liquid density, respectively. s and ω represent the number of rotor blades and the angular velocity of the turbine, respectively. Also, v_r and u_r are mean axial flow velocity and circumferential velocity, respectively; s indicates the area of each annular blade.

A flow simulation was carried out using the software of ANSYS Fluent 19.0, which uses the finite-element numerical method for solving the *Reynolds-averaged Navier-Stokes* equations by means of the pressure-based solver. The whole 3D geometry model of the turbine was established using ANSYS Workbench (specific parameter values can be obtained in Section 3.3), and grids were generated using the pre-processing software ICEM-CFD.

The k-ε reliable model is chosen as the fluid analysis model, the second-order upwind model is used for discretization, the simple solution algorithm is selected, and the pressure discretization scheme is presto. CFD simulation analysis model and meshing are shown in Fig.7, Fig.8 illustrates that the torque coefficient remains basically constant under the same flow coefficient when the number of mesh cells is greater than or equal to 4.68 million. Therefore, we chose to use a moderate number of mesh cells (4.68million) to save computing resources and improve work efficiency.

The impact torque and impact force of the turbine directly affect the start-up performance of the turbine [30]–[32]. The magnitude of the hydraulic torque determines whether the turbine can overcome the system load torque and the friction torque. Therefore, when the turbine works, it is not necessary to consider the hydraulic efficiency of the blades, and only the torque and impact force of the HBT are important. There are many factors affecting turbine performance. This paper uses CFD software to simulate and analyze the system of nozzle

TABLE 1. Eccentric platform design parameter.

Parameters	Value	Parameters	Value
r_2 (m)	0.11	r_{TB} (m)	0.081
r_1 (m)	0.045	μ_{TB}	0.0025
ρ(kg/m$^{3)}$	11000	P (MPa)	1
G(m/s^2)	9.8	S (mm^2)	2713
r_{AB} (m)	0.08375	r_{ab} (m)	0.054
μ_{AB}	0.0015	μ_P	0.2

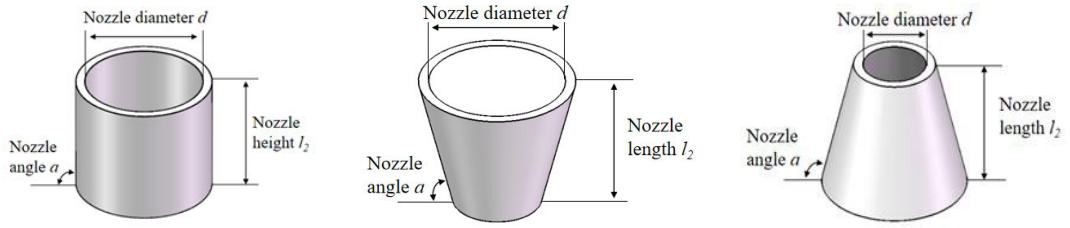

(a) Cylindrical nozzle (b) Shrinkage nozzle (c) Amplified nozzle

FIGURE 9. Different nozzle shapes, (a) Cylindrical nozzle, the nozzle diameter is constant and no boost is generated; (b) Shrinkage nozzle, the nozzle diameter is gradually reduced, resulting in supercharging; (c) Amplified nozzle, the nozzle diameter gradually becomes larger and produces a pressure drop.

and the HBT to explore the influence of different factors on the turbine force.

C. SIMULATION PARAMETERS OF CFD

In this paper, a novel HBT is installed at MVDS, the balance moment generated by the HBT is used to stabilize the upper disc valve at a predetermined position. The ''soft'' connection between the eccentric platform and the upper disc valve is realized, so that the eccentric platform is not affected by the friction resistance of the upper and lower disc valve.

The impact torque and impact force of the turbine directly affect the start-up performance of the turbine. The magnitude of the hydraulic torque determines whether the turbine can overcome the system friction torque, which drives the upper disc valve to rotate, and the impact force affects the system friction torque. Therefore, unlike conventional turbines, when the turbine works, it is not necessary to consider the hydraulic efficiency of the blades, and only the torque and impact force of the HBT are important. This paper uses computational fluid dynamics (CFD) software to simulate and analyze the system of nozzle and the HBT to explore the influence of different factors on the turbine force. A flowing fluid follows the law of conservation of mass, momentum and energy. However, it is very difficult to solve the velocity field and pressure field in complex flows accurately. The CFD method can be used to solve the approximate solution to satisfy the engineering application. The accuracy of CFD methods has been verified in many fields [33]–[35]. This paper employed numerical simulation tools to demonstrate the results of the theoretical analysis, and to study the variation of geometric parameters. The design of the eccentric platform in this paper takes the parameters as shown in the Table 1.

According to the structural parameters of the MVDS [15] and the design of the eccentric platform, the basic dimensions of the turbine are determined: the inner diameter is 44.5mm and the wall thickness is 2.75mm. The important factor in the design of HBT is the flow angle. Near the flow angle, the external force acting on the turbine changes dynamically. Therefore, the transient analysis is used to study the change of the force acting on the turbine when the nozzle is near the symmetrical position and under different flow angles.

Different nozzle shapes may affect the turbine toques. In this paper, the influence of three nozzle types on turbine performance is considered. Three turbine shapes are shown in Fig. 9. The influence of different nozzle shapes on turbine torques and impact forces are studied.

A flow simulation was carried out using the software of ANSYS Fluent 19.0, which uses the finite-element numerical method for solving the *Reynolds-averaged Navier-Stokes* equations [Eq.(23)] by means of the pressure-based solver. The whole 3D geometry model of the turbine was

TABLE 2. Optimized parameters design of turbines and nozzles.

Γ (°)	g (°)	w (mm)	h (mm)	l_1 (mm)	h_0 (mm)	v (m/s)	d (mm)	k (mm)	l_2 (mm)	Γ (°)
36	22.5	4	80	108	5	20	40	88	40	40

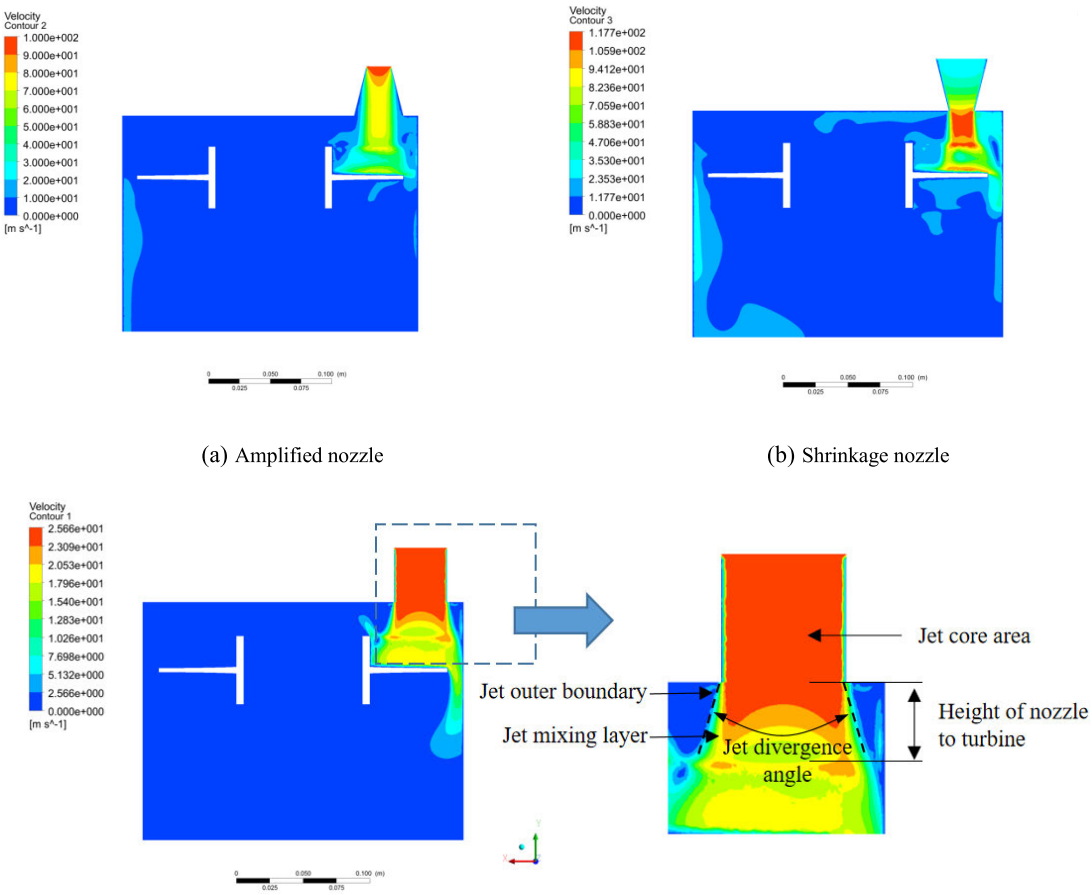

(a) Amplified nozzle

(b) Shrinkage nozzle

(c) Cylindrical nozzle

FIGURE 10. Velocity contour of different nozzle cross-section, (a) Amplified nozzle, shows the flow rate from high to low; (b) Shrinkage nozzle, shows the flow rate from low to high; (c) Cylindrical nozzle, the flow rate does not change much inside the nozzle, the fluid becomes unstable depending on the relative height of the nozzle and the turbine.

established using ANSYS Workbench (specific parameter values can be obtained in Table 2, No. represents the system parameters corresponding to different simulation tests), and grids were generated using the pre-processing software ICEM-CFD.

$$\begin{cases} \dfrac{\partial}{\partial x_i}(\vec{\mu}_i) = 0 \\ \dfrac{\partial u_i}{\partial t} + \dfrac{\partial}{\partial x_j}(u_i u_j) = -\dfrac{\partial P}{\rho \partial x_i} + \dfrac{\partial}{\partial x_j}[\dfrac{(u+u_t)}{\rho}(\dfrac{\partial u_i}{\partial x_j} + \dfrac{\partial u_j}{\partial x_i})] + f_i \end{cases} \tag{23}$$

where, P is pressure, ρ is fluid density, $\vec{\mu}_i$ is velocity vector, f_i is volume force vector, μ is dynamic viscosity.

IV. RESULTS AND DISCUSSION

A. DYNAMICS OF HBT

The design of experiments (DOE) method in the ANSYS Work-bench was employed to create a design space and Standard Response Surface-Full 2nd order polynomial model was used to study the influence of design variables on the turbine efficiency.

As shown in Fig.10 (a), the amplified nozzle jet diffuses at the inlet, the core area of the jet attenuates completely before the outlet of the nozzle, while the jet velocity of the shrinkage nozzle diffuses at the outlet of the nozzle, and the core area of the jet lasts until it contacts the turbine, as shown in Fig. 10 (b). Therefore, although the inlet velocity of amplified

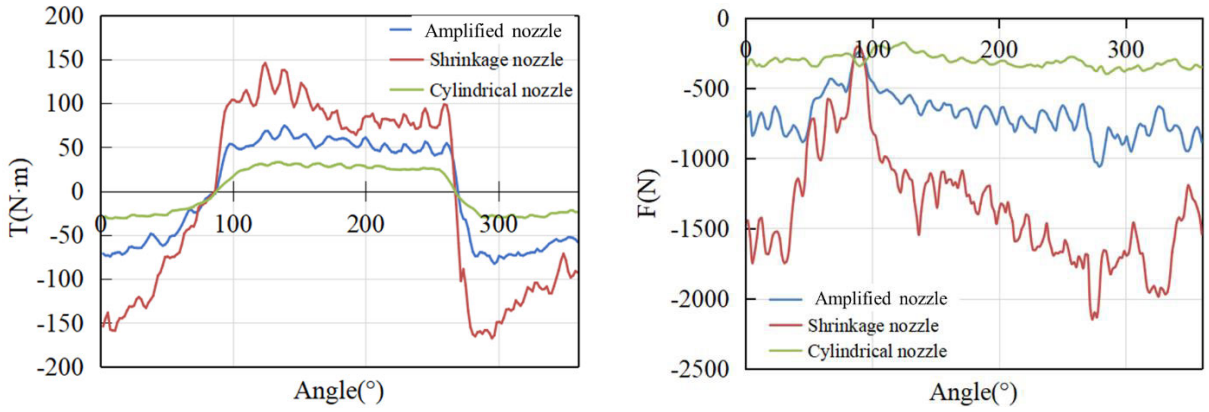

(a) Impact torque variation

(b) Impact force variation

FIGURE 11. Force variation of turbine with different nozzle shapes, when the nozzle rotates 360 degrees, in the situation of the same flow rate (a) shows the shrinkage nozzle produces the greatest impact torque, while the cylindrical produces the smallest; (b) shows the shrinkage nozzle produces the greatest impact force, while the cylindrical produces the smallest.

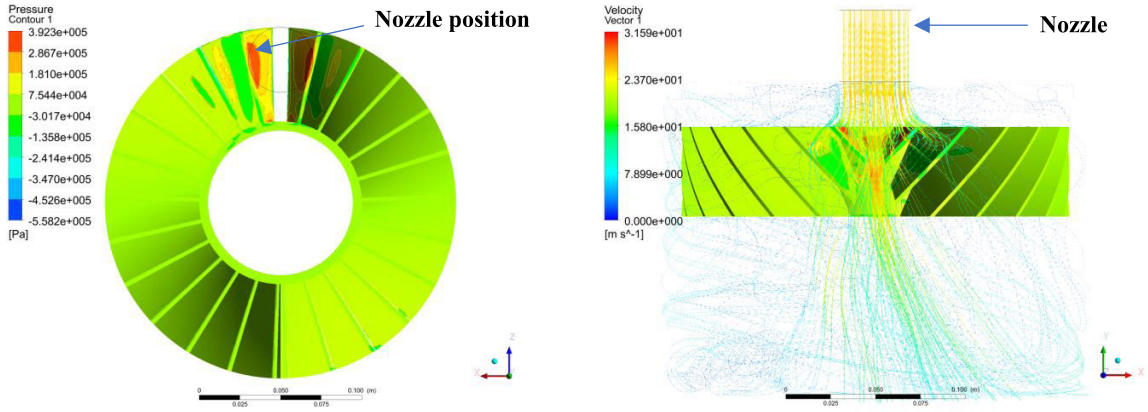

FIGURE 12. Pressure contour and velocity vector when turbine stops, left is the pressure contour and right is velocity vector. Steady state of HBT, balanced torque is stable and the system is converging.

nozzle is equal to the outlet velocity of shrinkage nozzle, the structure of the amplified nozzle leads to the decrease of jet average velocity, and finally the velocity of amplified nozzle jet impacting turbine is much lower than that of shrinkage nozzle, which leads to different toques on turbine. The force of the cylindrical nozzle is more stable than that of the other two nozzles, as shown in Fig.10 (c) which is due to the smaller velocity and the smaller turbulence fluctuation in the flow field. As shown in Fig.10 (c), the velocity distribution of the fluid is uniform when it just leaves the nozzle. After flowing a certain distance in the Y direction, the boundary of the jet becomes wider and wider, while the velocity of the jet decreases gradually, because the jet pumps and entrains a large amount of surrounding fluid. The jet boundary layer expands to both sides as the distance of the exit increases in the Y direction.

Torques and impact forces of turbines with different nozzles in different positions are shown in Fig. 11. The torque and impact force produced by the shrinkage nozzle are greater than that produced by the amplified nozzle at the same flow rate, while the cylindrical nozzle produces the least torque and impact force.

Considering the comprehensive torque and thrust, we choose the cylindrical nozzle as the practical application. In the following simulation and experimental results, we have adopted this structure. When the turbine is in a steady state, the final stop position of the turbine is as shown in Fig.12. At this time, the nozzle is in the balance position, and the turbine is balanced and stationary. When the balance is broken by disturbance, the turbine will provide a recovery torque.

Simulation study of different design parameters as shown in table 2, under the condition that other factors remain unchanged, that turbine blade angle γ, nozzle diameter d_0, blade thickness w, fluid velocity v, nozzle distance h_0 from the center of the turbine have impact on the torque of the turbine. We did 10 sets of simulation experiments, two of which are shown in the Fig.13. As shown in the Fig.13 (a),

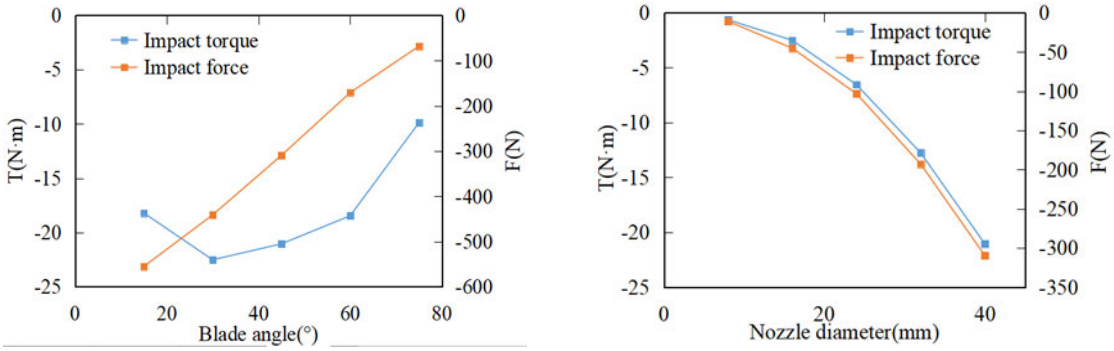

(a) (b)

FIGURE 13. Effect of different factors on turbine torques and impact forces, the turbine blade angle γ and nozzle diameter d, have a greater impact on the force and torque.

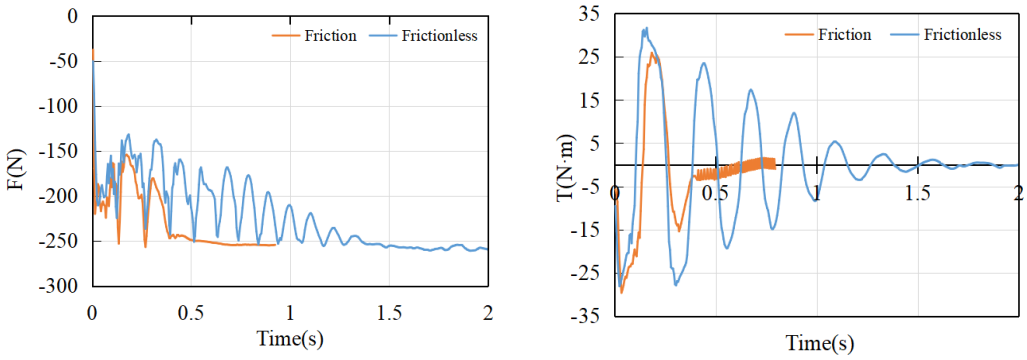

(a) Force variation (b) Torque variation

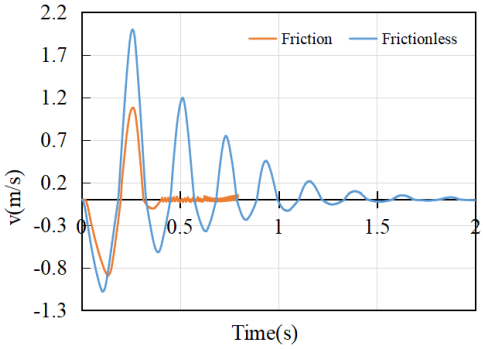

(c) Maximum tangential velocity variation

FIGURE 14. Turbine torque, force and maximum tangential velocity variations with or without friction, (a), (b), (c) shows the turbine oscillates continuously around the central axis, and its amplitude value of torque, force and maximum tangential velocity decreases continuously, eventually stabilized at a certain position; The stability time with friction is shorter than that without friction. And the fluctuation at the tail of curves in case of friction is caused by discontinuity of calculation due to time step.

we obtained the maximum torque value when blade angle is 36 degrees. With the increase of nozzle diameter d_0, fluid velocity v and distance k from the nozzle to the turbine center, the absolute value of the torque and impact force on the turbine increases (Fig.13 (b)). The turbine's parameter design should be determined according to the influence of different factors on start-up performance of the turbine. Turbine torque directly determines whether the turbine can overcome the friction torque to drive the upper disc valve. The impact force on the turbine results in the change of the friction force of the system. Different factors have different changes in the torque and impact force.

In the case of the presence or absence of friction, the torque, impact force and speed curve of the HBT stability

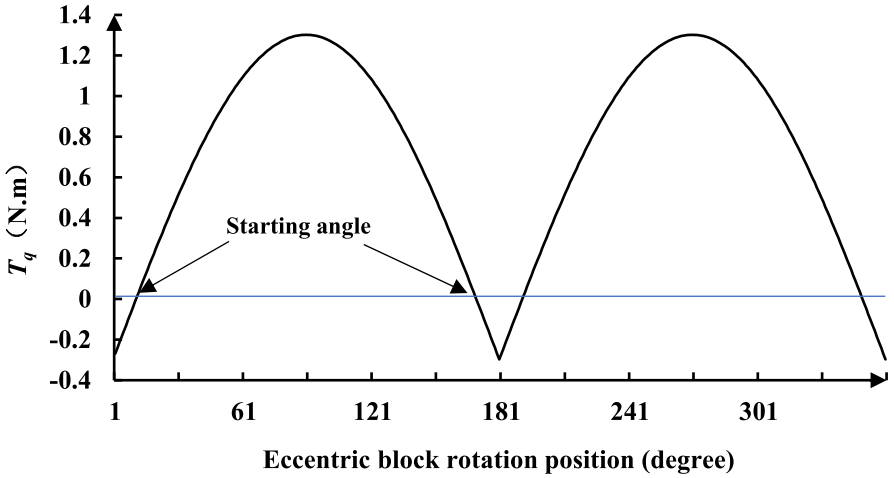

FIGURE 15. Torque difference Tq as the eccentric block rotates.

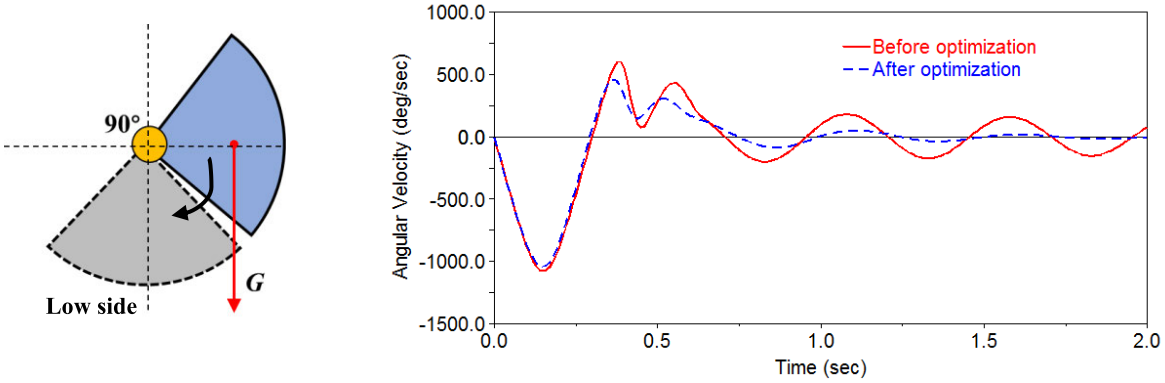

FIGURE 16. Angular velocity $\dot{\phi}$ for eccentric block before and after optimization by HBT, when the bottom drillstring does not rotate, the eccentric block rotates downward from 90° from the lower side.

process are shown in Fig. 14. The turbine oscillates continuously around the central axis and eventually stabilized at a certain location. Amplitude value of torque and maximum tangential velocity of the turbine decreases continuously to zero while the force gradually stabilizes to a fixed value. The amplitude of the torque changing with time decreases gradually and eventually becomes zero, which is consistent with the approximate linear variation of turbine torque near the flow angle mentioned above.

The curve of torque, force, and maximum tangential velocity of the turbine without friction is smoother while the curve with friction fluctuates at the tail. This is because the friction force will change abruptly when the velocity direction changes and the calculation is discontinuous due to the time step, which will lead to the instability of the turbine speed and the fluctuation of the turbine speed in the balance position. Turbine torque also fluctuates due to the fluctuation of turbine's position.

When designing the turbine blade, it is necessary to consider comprehensively so as to achieve the optimal relationship between the torque and the impact force. In principle, the greater torque of the turbine is better and the smaller force of the turbine is better. However, considering the strength and durability of the turbine, the turbine blade thickness was set to 4 mm and the fluid velocity was 20m/s. Considering the coupling relationship between the nozzle diameter and the nozzle from the center, when the nozzle diameter is 40 mm, the distance between the nozzle and the center of the turbine is preferably 88 mm. At the same time, the turbine design also needs to cooperate with the parameters of MVDS, borehole size, drilling pressure, drilling fluid type and so on. According the research above, optimized parameters design of the turbine is shown in Table 2.

B. OPTIMIZATION OF ECCENTRIC BLOCK DYNAMICS

The stable platform included an eccentric block which is not only sensitive to gravity, but also severely affected by vibration of drillstring [12], [15], [18]. When the eccentric torque of the eccentric block is greater than the friction torque of the bearing and the disc valve, the eccentric block can be started. At this time, the position of the corresponding lower side of the eccentric block is the critical start angle. Starting torque $T_q = T_E\text{-}T_f$, for different well inclination angles β, when the torque of the eccentric block is equal to the

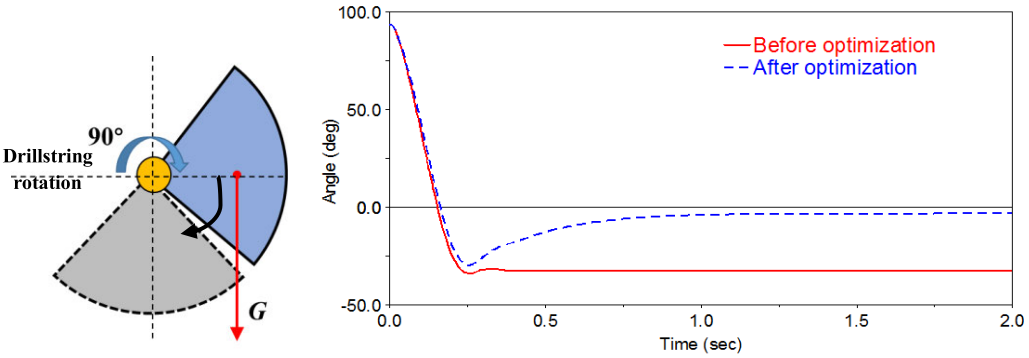

(a) The eccentric block starts at 90° when the drill string rotates clockwise

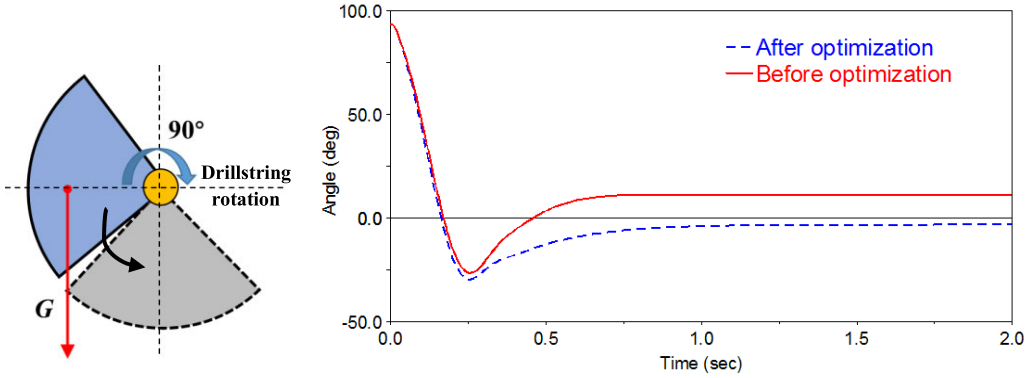

(b) The eccentric block starts at 90° when the drill string rotates counterclockwise

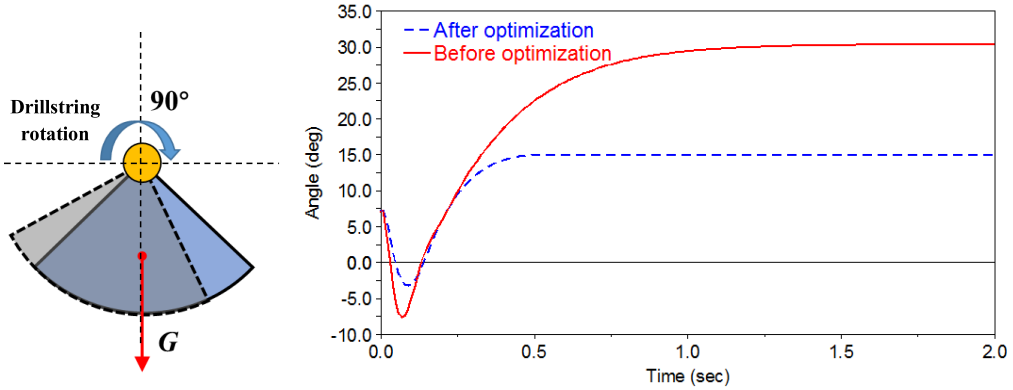

(c) The eccentric block starts at 7.5° when the drill string rotates clockwise

FIGURE 17. Rotation position ϕ curves of eccentric blocks at different starting positions.

frictional resistance, the angle φ between the eccentric block and the low side of the well is the starting angle.

As shown in the Fig. 15, when the well is inclined at 6 °, the change curve of T_q, the intersection point of the curve and the x-axis of the abscissa is the starting critical angle. It is convenient to explain that it cannot be started under the x-axis. The larger the value, the greater the startup acceleration.

When the bottom drillstring does not rotate, the eccentric block rotates downward from 90° from the lower side, as shown in the Fig.16 is the angular velocity $\dot{\phi}$ curve for eccentric block before and after optimization, after optimization of HBT, the eccentric block approaches the steady state faster.

Since the friction depends on the relative speed of movement, the rotation of the drillstring will greatly affect the stability of the eccentric block [15], the ''soft'' connection by HBT in this paper will play a more significant role. As shown in the Fig.17, when the eccentric block is in a different starting position, the rotation of the drillstring will greatly affect the

FIGURE 18. Prototype of MVDS and Eccentric block response test bench.

final stable angle of the eccentric block. As shown in the Fig.17, (a) when the starting direction of the eccentric block is the same as that of the drillstring, after the eccentric block falls to the low side, it continues to move to a specific angle due to the friction. After HBT optimization, the stable angle is closer to the low side, which can make the control of MVDS more accurate; (b) when the starting position of the eccentric block is opposite to the direction of rotation of the drill string, after the eccentric block falls to the low side, eccentric block rotation will reverse recovery in the direction of drillstring rotation. Before optimization, the stability angle will change due to different starting positions. After optimization, due to the use of a soft connection, the stability angle is largely unaffected by drill string motion. (c) assuming the starting position of the eccentric block is near (7.5° in the Fig.17.c) the low side, the rotation of the drill string will cause it to leave the original position. Although the friction of the bearing still exists after optimization, the eccentric block cannot be kept completely on the low side, but the swing amplitude is greatly reduced.

C. LABORATORY TEST TO VERIFY EFFECTIVENESS

The above simulations verify the effectiveness of the balanced turbine.

Additionally, we built a prototype to test the control accuracy of the proposed MVDS on the laboratory-scale. As shown in the Fig.18, is the prototype of MVDS and eccentric block response test bench. We can test the inductive accuracy of the eccentric block control mechanism in the laboratory, and objectively reflect the dynamic response of the eccentric control mechanism during the action.

During the test, the effects of the rotation of the drill string, the friction between the upper- and lower-disc valves and the bearings on the eccentric platform can be simulated, the rotation motion of the eccentric platform can be measured, and the final stability angle of the eccentric block can be recorded under different well deflection conditions. As the value of the circular hole of the upper valve θ can be adjusted according to different designs, therefore, during the work of the eccentric block, the stability angle of the eccentric block will determine the opening radius of the upper disc valve which is very important for the control accuracy.

We test that when the drill string is rotated, the eccentric block is at the starting position of 90 °, and the final stability angle is shown in the Fig.19. As the length of the eccentric block continues to increase, the stable angular position decreases. However, if the length of the eccentric block is too long, it will increase costs and cause new downhole problems. Based on the length of the eccentric block of 3.5m, the stability of the control angle was significantly improved after optimization with HTB. The high degree of fit between the calculated value and the laboratory test value indicates that the theoretical calculation is reliable.

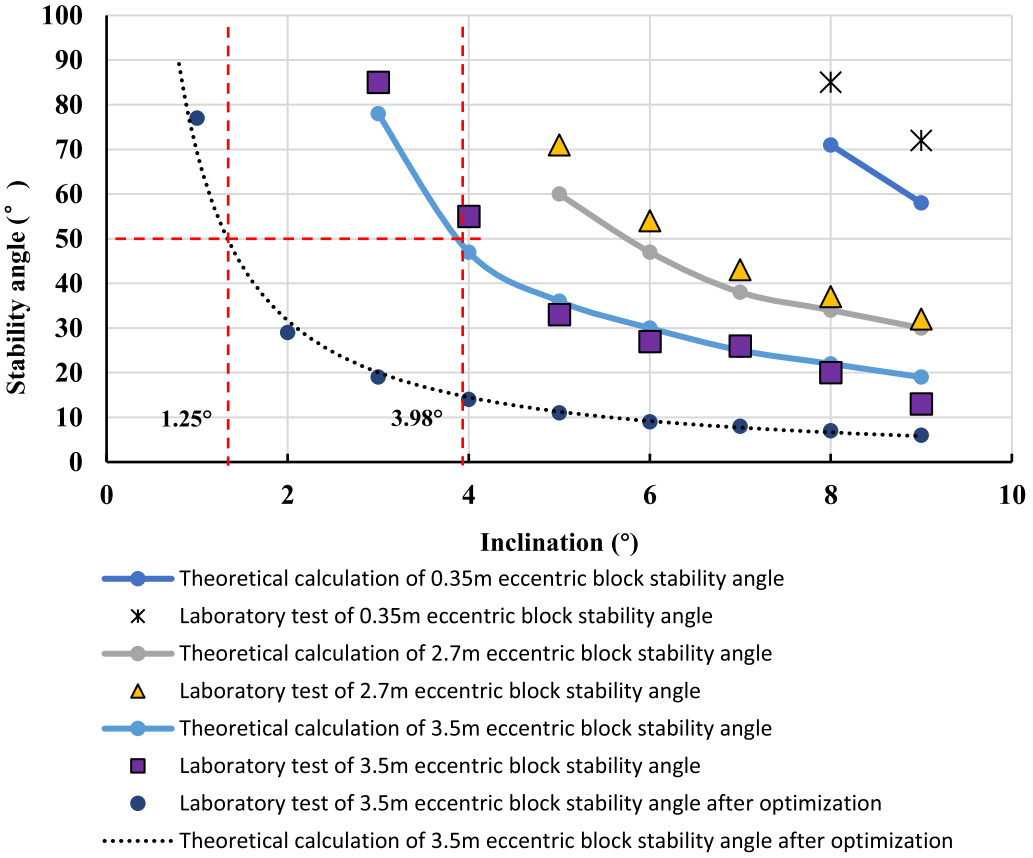

FIGURE 19. Eccentric block stability angle, experimental and theoretical comparison values, the theoretical and laboratory test have good consistency. As the length of the eccentric block increases, the position of the stable angle from the lower side becomes smaller and smaller. If the threshold of the stability angle in engineering application is not more than 50°, the 3.5m eccentric block needs 3.98 degree well deviation to respond before optimization, however, after optimization, the response accuracy has become 1.25 degrees, and the engineering applications have been greatly improved.

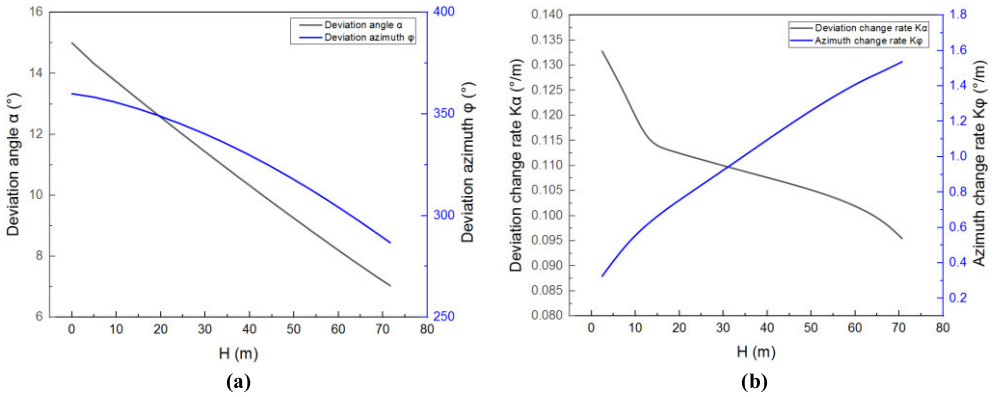

FIGURE 20. The value of deviation angle and azimuth angle gradually decreases (as shown in Figure b), and the borehole trajectory formed by drilling is a three-dimensional curve, which has the tendency of drifting to the left (as shown in Figure a).

This paper is about trying to improve the performance of a mechanical vertical-drilling tool (i.e. a tool to keep the hole vertical in the face of deflection forces). The main contribution of the paper is to add a novel turbine to the internal mechanism of vertical drilling tool. This turbine should allow the tool to be more effective – to keep the hole closer to vertical. Our experiment can only be carried out on the overall drilling tool to verify the work effect with or without HBT optimization.

The accuracy is not so good for the theoretical test related to the 0.35m eccentric block stability angle, that is because when the eccentric block is short, the eccentric gravity

acceleration is small, and the interference of friction, damping and other resistance plays a key role. These influencing factors cannot be fully considered in the theoretical model. Therefore, the error between theoretical calculation and experimental results is larger than when the eccentric block is longer.

D. INCLINATION AND AZIMUTH BUILDING CALCULATIONS

In the process of deviation correction, the value of deviation angle and azimuth angle gradually decreases (as shown in Figure 20.a), and the borehole trajectory formed by drilling is a three-dimensional curve, which has the tendency of drifting to the left [36]. Furthermore, the deviation change rate decreases and the azimuth change rate increases with the increase of vertical depth (as shown in Figure 20.b). That's because as the deviation angle decreases, the tool face angle of MVDS increases. Resulting in the pushing force distributed in the deviation plane decreases gradually, and the pushing force distributed in the azimuth plane increases gradually.

V. CONCLUSION

We proposed and developed a novel MVDS with high control accuracy in this paper. A new type of Hydraulic Balance Turbine (HBT) is presented and applied to the eccentric platform-disc valve mechanism used in MVDS. In MVDS, because of the friction resistance between the upper- and lower-disc valves and the vibration of the bottom drilling tool [18], [19], the deviation control accuracy of the MVDS is difficult to improve, which has become the main factor restricting its development.

The HBT is used to drive the upper disc valve to reduce the frictional resistance and the influence of the bottom drilling tool vibration on the bias platform to improve the control accuracy. This can achieve a ''soft'' connection between eccentric platform and the upper valves, eliminate the effect of the friction between the upper valve and the lower valve, and optimize the valve control ability. In this paper, the optimization mechanism of the HBT to control the mechanical performance of the MVDS disc valve mechanism is revealed. Torque and impact force acting on the HBT are the most important parameters affecting the performance of turbine. Turbine blade angle, nozzle diameter, blade thickness, fluid velocity and distance from nozzle center to that of the turbine have great influence on the turbine torque, which is the main factor to be considered in HBT design.

Through dynamics analysis of eccentric block, the rotation of the drillstring will greatly affect the final stable angle of the eccentric block. After HBT optimization, the stable angle is closer to the low side, which can make the control of MVDS more accurate. The same conclusion was verified by laboratory tests, As the length of the eccentric block increases, the position of the stable angle from the lower side becomes smaller and smaller. If the threshold of the stability angle in engineering application is not more than 50°, the 3.5m eccentric block needs 3.98 degree well deviation to respond before optimization, however, after optimization, the response accuracy has become 1.25 degrees, and the engineering applications have been greatly improved. However, in this study, we have assumed that the drillstring rotates at a uniform speed. In fact, the drillstring will exhibit complex dynamic forms of motion such as torsion, stick-slip, etc. Further research is required for in-depth analysis of the effect of the tool in mitigating torsional stick/slip vibrations.

REFERENCES

[1] T. Ma, P. Chen, and J. Zhao, ''Overview on vertical and directional drilling technologies for the exploration and exploitation of deep petroleum resources,'' *Geomech. Geophys. Geo-Energy Geo-Resour.*, vol. 2, no. 4, pp. 365–395, Dec. 2016.

[2] M. Reich, M. Oesterberg, H. Montes, and J. Treviranus, ''Straight down to success: Performance review of a vertical drilling system,'' in *Proc. SPE Annu. Tech. Conf. Exhibit.*, Oct. 2003, pp. 5–8.

[3] J. A. Short, *Introduction to Directional and Horizontal Drilling*. Tulsa, OK, USA: Pennwell Publishing Company, 1993.

[4] R. Emmermann and J. Lauterjung, ''The German continental deep drilling program KTB: Overview and major results,'' *J. Geophys. Res., Solid Earth*, vol. 102, no. B8, pp. 18179–18201, Aug. 1997.

[5] P. J. O'Brien, J. Duyster, B. Grauert, W. Schreyer, B. Stöckhert, and K. Weber, ''Crustal evolution of the KTB drill site: From oldest relics to the late Hercynian granites,'' *J. Geophys. Res., Solid Earth*, vol. 102, no. B8, pp. 18203–18220, Aug. 1997.

[6] J. Sugiura, A. Bowler, and R. Lowdon, ''Improved continuous azimuth and inclination measurement by use of a rotary-steerable system enhances downhole-steering automation and kickoff capabilities near vertical,'' *SPE Drilling Completion*, vol. 29, no. 2, pp. 226–235, Jun. 2014.

[7] T. Bratton, S. Edwards, J. Fuller, L. Murphy, S. Goraya, T. Harrold, J. Holt, J. Lechner, H. Nicholson, W. Standifird, and B. Wright, ''Avoiding drilling problems,'' *Oilfield Rev.*, vol. 13, no. 2, pp. 32–51, 2001.

[8] B. Comeaux, J. Gibb, K. Kirkhope, and P. Shaw, ''New automatic vertical drilling system for high temperature, harsh environment and performance drilling applications,'' in *Proc. Offshore Medit. Conf. Exhib.*, Ravenna, Italy, Mar. 2007, pp. 28–30.

[9] Q. Xue, R. Wang, B. Liu, and L. Huang, ''Dynamic measurement of spatial attitude at bottom rotating drillstring: Simulation, experimental, and field test,'' *J. Energy Resour. Technol.*, vol. 138, no. 2, pp. 1–9, Mar. 2016.

[10] B. Shang, Y. Ma, R. Hu, C. Yuan, J. Hu, and X. Luo, ''Passive thermal management system for downhole electronics in harsh thermal environments,'' *Appl. Thermal Eng.*, vol. 118, pp. 593–599, May 2017.

[11] P. Hagler, P. Henson, and R. W. Johnson, ''Packaging technology for electronic applications in harsh high-temperature environments,'' *IEEE Trans. Ind. Electron.*, vol. 58, no. 7, pp. 2673–2682, Jul. 2011.

[12] Q. Xue, H. Leung, R. Wang, B. Liu, L. Huang, and S. Guo, ''The chaotic dynamics of drilling,'' *Nonlinear Dyn.*, vol. 83, no. 4, pp. 1–16, 2016.

[13] J. Pippola, T. Marttila, and L. Frisk, ''Protective coatings of electronics under harsh thermal shock,'' *Microelectron. Rel.*, vol. 54, nos. 9–10, pp. 2048–2052, Sep. 2014.

[14] J. Steve, F. Chad, C. Juan, and S. Junichi, ''Fully mechanical vertical drilling system delivers RSS performance in vertical drilling applications while providing an economical alternative to conventional rotary steerable systems set-Up for vertical hold mode,'' in *Proc. IADC/SPE Drilling Conf. Exhib.*, Fort Worth, TX, USA, Mar. 2016, pp. 1–3.

[15] L. Li, Q. Xue, B. Liu, J. Wang, and X. Li, ''The dynamics of eccentric block in a fully mechanical vertical drilling tool under the effect of torsional vibration,'' *Adv. Mech. Eng.*, vol. 10, no. 4, pp. 1–18, 2018.

[16] D. Herrington and S. Mercer, ''Fully mechanical 3D rotary steering technology provides economical alternative to conventional rotary steerable tools,'' in *Proc. SPE Annu. Tech. Conf. Exhib.*, New Orleans, LA, USA, Oct. 2013.

[17] M. I. Khan, ''Falling oil prices: Causes, consequences and policy implications,'' *J. Petroleum Sci. Eng.*, vol. 149, pp. 409–427, Jan. 2017.

[18] Q. Xue, H. Leung, L. Huang, R. Zhang, B. Liu, and J. Wang, ''Modeling of torsional oscillation of drill-string dynamics,'' *Nonlinear Dyn.*, vol. 96, no. 1, pp. 267–283, 2019.

[19] L. Huang, Q. Xue, B. Liu, C. Yang, R. Wang, and L. Han, "Dynamic reliability analysis of rotary steering drilling system," *Mech. Sci.*, vol. 10, no. 1, pp. 79–90, Feb. 2019.
[20] M. Kapitaniak, V. V. Hamaneh, J. Páez Chávez, K. Nandakumar, and M. Wiercigroch, "Unveiling complexity of drill–string vibrations: Experiments and modelling," *Int. J. Mech. Sci.*, vols. 101–102, pp. 324–337, Oct. 2015.
[21] A. Bowler, L. Logesparan, J. Sugiura, B. Jeffryes, and M. Ignova, "Continuous high-frequency measurements of the drilling process provide new insights into drilling system response and transitions between vibration modes," *SPE Drilling Completion*, vol. 31, no. 2, pp. 226–235, 2016.
[22] R. Wang, Q. Xue, L. Han, F. Sun, and W. Yue, "Torsional vibration analysis of push-the-bit rotary steerable drilling system," *Meccanica*, vol. 49, no. 7, pp. 1601–1615, Jul. 2014.
[23] G. Dong and P. Chen, "A review of the evaluation, control, and application technologies for drill string vibrations and shocks in oil and gas well," *Shock Vibrat.*, vol. 2016, pp. 1–34, Oct. 2016.
[24] A. Guzek, I. Shufrin, E. Pasternak, and A. V. Dyskin, "Influence of drilling mud rheology on the reduction of vertical vibrations in deep rotary drilling," *J. Petroleum Sci. Eng.*, vol. 135, pp. 375–383, Nov. 2015.
[25] A. Ghasemloonia, D. Geoff Rideout, and S. D. Butt, "Analysis of multimode nonlinear coupled axial-transverse drillstring vibration in vibration assisted rotary drilling," *J. Petroleum Sci. Eng.*, vol. 116, pp. 36–49, Apr. 2014.
[26] Y. T. Feng and D. R. J. Owen, "Discrete element modelling of large scale particle systems—I: Exact scaling laws," *Comput. Part. Mech.*, vol. 1, no. 2, pp. 159–168, Jun. 2014.
[27] D. Luo, X. Tan, and D. Huang, "Design and performance analysis of three stage centrifugal turbine," *Appl. Thermal Eng.*, vol. 138, pp. 740–749, Jun. 2018.
[28] S. Rehman, M. Alam, L. Alhems, and M. Rafique, "Horizontal axis wind turbine blade design methodologies for efficiency enhancement—A review," *Energies*, vol. 11, no. 3, p. 506, Feb. 2018.
[29] M. Caboni, M. S. Campobasso, and E. Minisci, "Wind turbine design optimization under environmental uncertainty," *J. Eng. Gas Turbines Power*, vol. 138, no. 8, pp. 1–13, Aug. 2016.
[30] T. Suzuki and H. Mahfuz, "Analysis of large-scale ocean current turbine blades using fluid–structure interaction and blade element momentum theory," *Ships Offshore Struct.*, vol. 13, no. 5, pp. 451–458, Jul. 2018.
[31] R. MacNeill and D. Verstraete, "Blade element momentum theory extended to model low Reynolds number propeller performance," *Aeronaut. J.*, vol. 121, no. 1240, pp. 835–857, Jun. 2017.
[32] D. H. Hodges, "An extension of blade element momentum theory to incorporate nonlinear lift and drag coefficients," *J. Amer. Helicopter Soc.*, vol. 25, no. 4, pp. 48–50, Oct. 1980.
[33] M. M. Aslam Bhutta, N. Hayat, M. H. Bashir, A. R. Khan, K. N. Ahmad, and S. Khan, "CFD applications in various heat exchangers design: A review," *Appl. Thermal Eng.*, vol. 32, pp. 1–12, Jan. 2012.
[34] Y. Wang, K. Williams, M. Jones, and B. Chen, "CFD simulation methodology for gas-solid flow in bypass pneumatic conveying—A review," *Appl. Thermal Eng.*, vol. 125, pp. 185–208, Oct. 2017.
[35] P. Halder, A. Samad, and D. Thévenin, "Improved design of a wells turbine for higher operating range," *Renew. Energy*, vol. 106, pp. 122–134, Jun. 2017.
[36] L. Chai, K. Zhang, D. Yang, B. Liu, and D. Zhang, "Integral modeling for deviation correction trajectory of the mechanical vertical drilling system," *Machines*, vol. 9, no. 8, p. 161, Aug. 2021.

JIN WANG was born in 1986. He received the bachelor's degree in mechanical manufacturing and automation and the master's degree in mechanical manufacturing and automation from Zhejiang University, in 2008 and 2011, respectively. He is currently pursuing the Ph.D. degree in geological engineering with the China University of Geosciences. He has been worked as an Engineer at Beijing CSR Times Locomotive and Rolling Stock Mechanics Company Ltd., from 2011 to 2014. From 2014 to 2016, he has been worked at Bazhou DaPu Petroleum Technology Service Company Ltd. He has been researching on underground vertical drilling tools since he has been entering the China University of Geosciences, in 2016.

QILONG XUE was born in 1983. He received the bachelor's degree in electrical engineering and the Ph.D. degree in drilling engineering from the China University of Petroleum (East), in 2006 and 2014, respectively. He has been worked at China Petroleum Ltd., from 2006 to 2008. He has been engaged in research on measurement and control technology of drilling engineering. From September 2012 to September 2013, he was a Joint Researcher at the University of Calgary, where he focuses on research of real time measurement of bottom drilling tool's attitude and rotary steerable drilling systems. He is currently an Associate Professor with the China University of Geosciences.

BAOLIN LIU was born in 1959. He received the Ph.D. degree in engineering from the China University of Geosciences, Beijing. He is currently a Professor and the Director of the Key Laboratory on Deep Geodrilling Technology, Ministry of Land and Resources. His research interests include scientific drilling, environmental science drilling, computer controlled drilling, and new technology drilling engineering. He is a member of the professional committee of mineral exploration engineering.

FANGTAO LI was born in 1995. He is currently pursuing the master's degree with the China University of Geosciences, Beijing.

YANBIN ZANG was born in 1984. He received the Ph.D. degree in drilling engineering from the China University of Petroleum (East), in 2011. He is currently a Researcher and the Director of the Drilling Technology Research Institute of Sinopec Engineering Technology Research Institute. He has published more than 40 papers and authorized five invention patents. His research interests include shale oil and gas drilling technology.

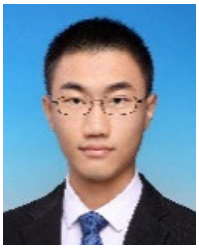

LIN CHAI was born in 1992. He received the bachelor's degree in petroleum engineering and the master's degree in drilling engineering from the China University of Petroleum, Beijing. He is currently pursuing the Ph.D. degree in geological engineering with the China University of Geosciences, Beijing.